Thesis for the degree of Licentiate of Engineering

Microwave Measurement Systems for Parameter Estimation and Classification

Johan Winges

CHALMERS

Department of Signals and Systems
Signal Processing Group
chalmers university of technology
Göteborg, Sweden, 2014

Microwave Measurement Systems for Parameter Estimation and Classification
JOHAN WINGES

Technical Report No. R009/2014, ISSN 1403-266X
Department of Signals and Systems
Signal Processing Group
Chalmers University of Technology
SE-412 96 Göteborg, Sweden, 2014
Telephone: +46 (0)31-772 1000

Cover:
Photograph of a tomography measurement system with superimposed electric field solution when the rightmost waveguide is excited. Here, an acrylic glass cylinder is positioned at the center of the measurement region and the electric field is computed at the frequency 4.0 GHz.

This thesis has been prepared using LaTeX

Printed by Chalmers Reproservice
Göteborg, 2014

There is a computer disease that anybody
who works with computers knows about.
It's a very serious disease and it
interferes completely with the work.
The trouble with computers is
that you 'play' with them!

Richard P. Feynman

ABSTRACT

Microwave measurement systems are attractive for diagnostics and monitoring purposes in a number of important applications. For example, the strong interaction between microwaves and water make microwaves well-suited for moisture measurements. Moreover, the power used in microwave measurements is often sufficiently low such that the measurement can be classified as non-destructive. As such, microwave measurements systems are appropriate for applications in, for example, biomedical imaging and monitoring of pharmaceutical processes.

In this thesis, parameter estimation methods are employed for two microwave measurement systems with application in the pharmaceutical industry. Additionally, we present a numerical study of a simplified microwave measurement system for the localization of intracranial bleedings via classification. In order to achieve good agreement between measured and simulated data, we utilize accurate electromagnetic models by means of the finite element method and calibration methods using a reference case measurement. In addition, we utilize a priori information to mitigate problems associated with parameter ambiguity, where the a priori information may be incorporated by means of regularization.

First, we consider a transmission/reflection tomography measurement system. Here, the parameter estimation method involves a goal function that corresponds to the misfit between the measured and simulated scattering data, where a non-linear gradient-based optimization method is used to determine the parameters. The gradients are computed by means of continuum sensitivity expressions based on an adjoint field problem. The tomography system is used to estimate the effective permittivity of densely packed microcrystalline cellulose (MCC) pellets and we find that the estimated permittivity depends on the moisture content of the MCC pellets.

Second, we solve a minimization problem for resonance measurements in a pharmaceutical process vessel, which acts as a metal cavity. Here, we estimate parameters using a quadratic minimization problem with a regularization term, which incorporates a priori information provided from other sensors. The physical model is linearized and small perturbations of the resonant frequencies are related to small variations in the permittivity. During operation, the vessel is loaded with MCC pellets that are fluidized and circulated by injection of air, which yields a dilute MCC/air mixture. The measured resonant frequencies are used to estimate the effective complex permittivity of three different sub-regions inside the process vessel as a function of process time.

Keywords: microwave measurements, parameter estimation, finite element method, gradient-based optimization, sensitivities, microcrystalline cellulose, permittivity

LIST OF APPENDED PAPERS

Paper I L. Cerullo, J. Winges, T. Rylander, J. Nohlert, T. McKelvey, L. Gradinarsky, S. Folestad and M. Viberg, **"Microwave Measurement System for Dispersive Dielectric Properties of Densely Packed Pellets,"** submitted to Measurement Science and Technology.

Paper II L. Cerullo, J. Nohlert, J. Winges, T. Rylander, T. McKelvey, L. Gradinarsky, M. Viberg and S. Folestad, **"Microwave Measurements for Metal Vessels,"** *Proceedings of the 7th European Conference on Antennas and Propagation, EuCAP 2013*, 2013.

Paper III J. Nohlert, L. Cerullo, J. Winges, T. Rylander, T. McKelvey, A. Holmgren, L. Gradinarsky, S. Folestad, M. Viberg, A. Rasmuson, **"Global Monitoring of Fluidized-Bed Processes by means of Microwave Cavity Resonances,"** submitted to Measurement.

Paper IV S. Candefjord, J. Winges, Y. Yu, T. Rylander, T. McKelvey, **"Microwave technology for localization of traumatic intracranial bleedings – A numerical simulation study,"** *Proceedings of the 35th International Conference on Engineering in Medicine and Biology Society, EMBC'13*, 2013.

ACKNOWLEDGMENTS

I would like to express my gratitude to a number of people. Your help and support have been greatly appreciated during the last years.

First, my main supervisor Thomas Rylander. I thank you for the opportunity to become a PhD student. I am really enjoying it so far! Also, thanks for guiding, discussing and educating me in what it means to be a researcher.

A special thanks to Livia Cerullo and Johan Nohlert. It has been a pleasure getting to know and working with you!

My current and former colleagues and friends in the Signal Processing group and the department of Signals and Systems.

Of course, my family. You have wholeheartedly supported me in pursuing higher education, and giving me the courage to believe I can succeed.

Finally, Jessica. Thank you for your love and support.

This PhD position is financially supported by the Swedish Research Council. Computations were performed on resources at Chalmers Centre for Computational Science and Engineering (C3SE) provided by the Swedish National Infrastructure for Computing (SNIC). Astra Zeneca is acknowledged for the support in terms of experimental data and measurement campaigns featured in this thesis.

Johan Winges
April, 2014

CONTENTS

CHAPTER 1

INTRODUCTION

The applications of microwaves are numerous and some examples of application areas are radar systems, astronomy, telecommunication systems and heating. The focus of this thesis is on microwave measurement systems, where the objective is to measure electrical material parameters and related quantities. In particular, this thesis explores the usage and benefits of accurate simulation tools in combination with extensive numerical computations for the modeling of microwave measurement systems and the corresponding development of computer algorithms for parameter estimation and classification.

1.1 Microwave Measurements

Microwave measurements offer competitive measurement techniques in many applications. We refer to Nyfors and Vainikainen [1] for a survey as well as classification of various types of microwave sensors for applications in industry, in medicine and for research purposes. The classes of microwave sensors are (i) resonance sensors, (ii) transmission sensors, (iii) reflection sensors, (iv) radar sensors and (v) special sensors such as radiometer sensors and active imaging systems.

As microwaves interact strongly with water, one fruitful application field is humidity and moisture measurements. An example is the microwave humidity sensor for difficult environments by Toropainen et al. [2]. This measurement system exploits the resonant[1] behavior of microwave cavities, and uses the measured resonant frequency shift (around 9.5 GHz) to estimate the air humidity given the air temperature inside the sensor. A possible limitation of the sensor is that the air and its temperature is assumed to be homogeneous. Another example is the low cost microwave sensor[2] for moisture content measurement in the paper milling industry by Gentili et al. [3]. From measuring the resonant frequency (around 0.85-0.95 GHz), they estimate the moisture content via an

[1]The sensor consists of an open ended cylindrical cavity resonator operating the TE_{011}-mode.
[2]The sensor is a 2-port cavity backed slot resonator.

inversion procedure on an artificial neural network trained on measurement data. Here, the measured resonant frequency is affected by (i) the thin gap of air between the sensor and the sheet of paper, (ii) the sheet's surface roughness, (iii) the thickness of the sheet and (iv) the moisture content. This yields a problem with multiple parameters with limited distinguishability.

Other interesting application fields are found in biomedical imaging, for example microwave breast imaging systems for detection of malignant tissue [4] or microwave brain imaging for stroke detection [5]. One breast imaging system is proposed by Winters et al. [6]. The presented measurement system consists of an array with five elliptical rings, where each ring contains eight electrically small dipole antennas. It measures the transmitted signal between all possible antenna pairs for a number of discrete frequencies between 0.5 GHz and 3.5 GHz. In the reconstruction of the image, they use smooth patient specific[3] basis functions instead of a mesh based material discretization as in Ref. [7]. They find that this approach significantly reduces the number of degrees of freedom in the reconstruction problem.

In most applications, a major advantage of microwave measurement techniques is that they are non-destructive[4]. In addition, microwaves have the ability to perform non-intrusive measurements, e.g. without contact with the measurement region, and that microwaves penetrate many materials. Also, microwave measurement equipment can be a portable and low-cost alternative as compared to other competing techniques. A possible disadvantage of microwave measurements is the simultaneous dependence of many parameters, such as temperature, density, size, position, moisture, etc., for applications where only a selection of these quantities is of interest to measure and the others are unknown. The possible spatial resolution in microwave imaging also depends on the wavelength of the microwaves. This makes details with small dimensions as compared to the wavelength difficult to resolve. Further, microwaves often have reduced penetration depth into materials with conductive losses as the frequency is increased.

For measurements based on microwaves we need (i) a network analyzer (or similar measuring device) to generate and measure the microwave signal, (ii) one or several antennas or probes connected to the network analyzer and (iii) a measurement region containing the object/material we would like to measure. The network analyzer generates a microwave signal which propagates along a transmission line to a connected antenna. The antenna radiates the microwave signal as an electromagnetic wave. The wave propagates into the measurement region, interacts with the measurement object, and is scattered. The scattered field is then measured by the network analyzer using either the same antenna that transmitted the wave (i.e. reflection) or by a different antenna (i.e. transmission). The network analyzer measure the (complex) reflection or transmis-

[3]The shape of the patients breast is considered known and used in the construction of the patient specific basis functions. The basis functions are constructed by introducing Gaussian functions on the subregions of a grid spanning the interior of the breast volume. In addition to a basis function representing the mean value, they generate (using a singular value decomposition) a minimal set of orthonormal basis functions, corresponding to spatial variations around the mean.

[4]In these applications, the necessary amount of power is sufficiently low to classify the microwave radiation as non-destructive or unharmful.

sion parameters. These parameters are found by comparing the amplitude and phase of the received signal with the transmitted signal for one frequency at a time.

For systems with N_p ports, the so-called scattering parameters $S_{p,q}(f)$ describe the received signal on port p given that a signal is transmitted into (only) port q for the frequency f, where $p = 1, \ldots, N_\mathrm{p}$ and $q = 1, \ldots, N_\mathrm{p}$. Note that for passive systems, the scattering parameters are complex numbers with a magnitude that does not exceed unity. The scattering parameters are usually stored in the scattering matrix $\mathbf{S}(f)$, where the row index corresponds to the receiving port index and the column index to the transmitting port index. In particular, we have the reflection coefficient on port p for $p = q$ (i.e. the diagonal of $\mathbf{S}$). Similarly, we have the transmission coefficient from port q to port p for $p \neq q$ (i.e. the off-diagonal elements in $\mathbf{S}$).

1.2 Numerical Methods for Electromagnetics

To interpret the measured scattering parameters, a model of the measurement system with its measurement region is necessary. In the measurement system, we propagate electromagnetic waves, which are described by the theory of classical electromagnetism. An introduction to the theory of electromagnetism can be found in the book by Cheng [8]. The theory of electromagnetism is expressed by Maxwell's equations[5], which can be used to create a physical model of the measurement system. In the physical model, the geometry and the electromagnetic properties of the materials influence the propagation and scattering of the electromagnetic wave.

There are a number of computational methods for solving electromagnetic field problems. The most popular methods are the finite-differences time-domain (FDTD) scheme, the finite element method (FEM) and the method of moments (MoM). These techniques have different advantages and disadvantages as they are compared to each other, and none is superior for all electromagnetic problems. An introduction to these numerical methods for electromagnetism can be found in the textbook [10].

The FDTD scheme is extensively used and it was introduced 1966 by Yee [11]. In the FDTD scheme, a finite-difference approximation of Maxwell's equations is employed on a structured grid, where the most common choice is a Cartesian grid. The straightforward discretization procedure yields a scheme that is easy to understand and implement. Moreover, a FDTD solver does not need to explicitly store the three-dimensional grid or a system matrix, which reduces memory requirements. However, curved or oblique boundaries are approximated by "stair-cases" due to the brick-shaped nature of the computational grid. Local refinement of the element size is unsupported by the standard scheme, making fine geometric details computationally expensive to model accurately.

The MoM, or the boundary element method, is based on integral formulations of Maxwell's equations [12]. In the MoM, the boundaries between different media are normally discretized. The field solution is not expressed explicitly in the MoM. Instead, we use the sources to the field as the unknowns. The field solution is then expressed by means of superposition integrals of the discretized sources, which involve a so-called

[5]Named so in respect to J. C. Maxwell's contributions in his paper published 1865 [9], finalizing the classical theory of electromagnetism.

Green's function. The system matrix produced by the MoM is in general a full matrix, which describes how the unknown sources on the discretized boundaries affect each other.

1.2.1 Finite Element Method

The finite element method is, like the FDTD scheme, a volume discretizing method and it was featured in applications in structural engineering already in the 1940's. The finite element method was adapted to work well in electromagnetic applications with the introduction of the edge-basis functions[6] by Nédélec in the 1980's [13]. Today, the FEM is an important numerical method for solving a large group of problems related to electromagnetism and numerous software packages exist. An introduction to the FEM in electromagnetics is found in the book by Jin [14].

The FEM discretizes the computational region into a mesh of finite elements of usually tetrahedral or hexahedral type in three dimensions and triangular or quadrilateral type in two dimensions. Moreover, the elements can be made smaller in regions where the solution varies rapidly, such as around field singularities at sharp edges and corners. A suitable set of basis functions is defined on the elements and the field solution is expressed as a linear combination of these basis functions with unknown coefficients. The solution is then found in a weak sense by setting the weighted residual of the differential equation to zero. In the FEM, a sparse[7] system matrix is constructed, which describes the local behavior of the field.

The most important advantage of the FEM in comparison to the FDTD scheme is its ability to mesh arbitrary curved and oblique boundaries. Further, fine geometric details are possible to model in FEM by reducing the mesh size locally. The FEM is, however, more memory expensive than the FDTD scheme as the mesh and the system matrix is normally explicitly stored. In comparison to the MoM, the system matrix in the FEM is sparse, which significantly reduce the computational burden and advocate for the use of efficient iterative solvers.

The basis functions employed in the FEM are often of polynomial type with some order p. Here, $p = 1$ corresponds to a linear variation across an element, $p = 2$ quadratic variation and so forth. Using a higher-order polynomial for the basis functions can in some cases significantly improve the solution approximation at a similar computational cost as compared to linear basis functions. As the local polynomial degree of the basis function is increased, the approximate solution can more easily represent smooth fields, which makes it possible to use larger elements. A finite element solver for an arbitrary order $p \leq 10$ is implemented for the Helmoltz equation and described in Sec. 3.1.1. This solver is utilized in **Paper I**, **Paper II** and **Paper IV**.

[6] The edge-basis functions provided an excellent solution to problems related to spurious solutions and field singularities around sharp geometrical features.

[7] In the FEM, we generally construct basis functions with local support. This makes only a few basis functions interact with each other, resulting in a sparse linear system of equations.

CHAPTER 2

PARAMETER ESTIMATION AND CLASSIFICATION

Many different types of parameter estimation techniques are used to relate measured quantities to sought quantities. In some cases, the measurement procedure can be trivial, such as when we determine the length of an object using a ruler, where we simply read the value directly from the ruler. In many applications, however, the quantity of interest influences the directly measured value in a complicated manner and, thus, we need a model that relates the measured quantities to the sought quantities, or vice versa. Such a model can, for example, be a physical model based on appropriate equations describing the system in terms of first principles, or an empirical model created from measurement data. We refer to the book by Aster et al. [15] for further details about parameter estimation and the broader subject of inverse problems. In this thesis, the focus is on parameter estimation using physical models derived from Maxwell's equations. Thus, we attempt to relate the measured electromagnetic quantities, such as the scattering parameters, to the dielectric properties and/or geometric dimensions of the measured object. The estimated dielectric properties can then be used to characterize a material in terms of other quantities, such as its moisture content.

Typically, a goal function is minimized in order to find an optimal parameter configuration that fits the measurement situation. The act of minimizing the goal function is often referred to as optimization, which is described next. An alternative approach to parameter estimation (in characterizing the measurement situation) is classification, which is described briefly at the end of this chapter.

2.1 Goal-Oriented Optimization

Given that the measured quantity is the scattering matrix $\mathbf{S}^{\mathrm{M}}$ at the specified frequency and the physical model of the scattering matrix is $\mathbf{S}(\mathbf{p})$, where $\mathbf{p}$ are some parameters defining the dielectric properties and/or geometric dimensions of the unknown object, a goal function can be constructed as

$$g(\mathbf{p}) = ||\mathbf{S}(\mathbf{p}) - \mathbf{S}^{\mathrm{M}}||\,, \tag{2.1}$$

where $||\cdot||$ is an appropriate norm. Here, Eq. (2.1) describes the misfit between the measured scattering matrix and the computational model of the scattering matrix in the specified norm.

The scattering matrix is a square matrix (e.g. N_{p}^2 elements) that can be measured for N_{f} frequencies. As such, the scattering data can be stored as a three-dimensional array. To simplify the mathematical description and treatment of the problem, we introduce $\mathbf{s}^{\mathrm{M}}$ and $\mathbf{s}(\mathbf{p})$ as the respective vectorized (one-dimensional) scattering data arrays for a set of discrete frequencies. In the following, we use a weighted norm for the goal function

$$g_{\mathbf{W}}^2(\mathbf{p}) = \left(\mathbf{s}(\mathbf{p}) - \mathbf{s}^{\mathrm{M}}\right)^H \mathbf{W} \left(\mathbf{s}(\mathbf{p}) - \mathbf{s}^{\mathrm{M}}\right) = ||\mathbf{s}(\mathbf{p}) - \mathbf{s}^{\mathrm{M}}||_{\mathbf{W}}^2\,, \tag{2.2}$$

where ^{H} is the Hermitian (complex conjugate transpose) operator and $\mathbf{W}$ is a diagonal matrix with real positive weights on the diagonal. An alternative goal function is $g_{\mathbf{W}}(\mathbf{p}) = \sqrt{g_{\mathbf{W}}^2(\mathbf{p})}$, which can be directly interpreted as the weighted root-mean-square (RMS) value of the misfit in the scattering parameters. An example of a weight matrix is $\mathbf{W}_0 = N_{\mathrm{p}}^{-2} N_{\mathrm{f}}^{-1}\mathbf{I}$, where the corresponding goal function $g_{\mathbf{W}_0}^2(\mathbf{p})$ is the mean-squared-deviation (MSD) between the physical model and the measurement data

For certain measurement systems, the electromagnetic problem features resonances with high Q-values. Here, the scattering parameters can be represented in terms of the resonant frequencies ω_i, for $i = 1, 2, \ldots$. Using for example a subspace-based multivariable system identification algorithm [16], we can estimate complex resonance frequencies ω_i^{M} for $i = 1, \ldots, N_\omega$ from measured scattering data $\mathbf{s}^{\mathrm{M}}$. A goal function formulation can be constructed for the estimated resonant frequencies $\boldsymbol{\omega}^{\mathrm{M}}$ and a corresponding physical model $\boldsymbol{\omega}(\mathbf{p})$, which is similar to Eq. (2.2) for the scattering parameters.

The parameter vector $\mathbf{p}$ is determined by the minimization of $g(\mathbf{p})$, which is what we denote as goal-oriented optimization. Typically, the scattering parameters depend non-linearly on the parameters $\mathbf{p}$. Thus, minimizing $g(\mathbf{p})$ in Eq. (2.2) is, in general, a non-linear and non-convex problem. Moreover, the parameters $\mathbf{p}$ can be subject to some, possibly non-linear, constraints. Optimization algorithms can be utilized to minimize $g(\mathbf{p})$. A common feature of many optimization algorithms is to use the sensitives of $\mathbf{s}(\mathbf{p})$ around the current point $\mathbf{p}_k$ to find a nearby point $\mathbf{p}_{k+1}$ that yields a reduced value of the goal function. The focus of the Sec. 2.1.1 is the use of the sensitivities of $\mathbf{s}(\mathbf{p})$, or gradients, with respect to $\mathbf{p}$ as we minimize $g(\mathbf{p})$.

In some measurement situations, the expected variation of the parameters $\mathbf{p}$ can be assumed small. If so, the computed quantity $\mathbf{s}(\mathbf{p})$ can be approximated to linearly depend on the parameters $\mathbf{p}$. The minimization problem can then be reduced into a quadratic problem, where the solution satisfies a system of linear equations. We describe this approach in detail in Sec. 2.1.2.

As the scattering parameters depend non-linearly on the parameters $\mathbf{p}$, the goal function $g(\mathbf{p})$ can have many local optima. To find a sufficiently good initial guess for a gradient-based optimization algorithm, a parameter study for a set $\mathbb{P}$ of parameter vectors $\{\mathbf{p}_1, \ldots, \mathbf{p}_N\}$ is executed and the computed result $\mathbf{s}(\mathbf{p}_i)$ is stored in a database $\forall \mathbf{p}_i \in \mathbb{P}$. The computation of a database is straightforward, parallelizable, and can be executed prior to any measurement of scattering data. However, the computational cost to compute and store a database grows exponentially with the number of parameters in the database. In particular, if the parameter vector $\mathbf{p}_i$ consists of N parameters, and a Cartesian grid with N_g points for each of the parameters is employed, the computational cost and storage requirements scale as N_g^N. The computation of databases is described in Sec. 2.1.3, together with other possible areas of usage.

2.1.1 Gradient-Based Optimization

Gradient-based optimization algorithms exploit an iterative scheme to minimize the goal function using the negative gradient as the search direction. The algorithm starts at the initially ($k = 0$) supplied guess $\mathbf{p}_k$ and evaluates the goal function $g(\mathbf{p}_k)$ and its gradient $\nabla_\mathbf{p} g(\mathbf{p}_k)$. For global convergence in a non-convex problem, the initial guess must be sufficiently close to the global minimum. In each subsequent iteration, the algorithm attempts to improve the parameter vector along the line $\mathbf{p}_{k+1} = \mathbf{p}_k - \nu \Delta \mathbf{p}$, where $\Delta \mathbf{p}$ is the direction given by the gradient and ν is the step length [17]. Here, ν is selected such that $g(\mathbf{p}_{k+1}) \leq g(\mathbf{p}_k)$, where a so-called line search often is employed. The algorithm continues to evaluate the goal function and its gradient until the termination criteria are fulfilled. The derivative of $g^2_\mathbf{W}(\mathbf{p})$ in Eq. (2.2) with respect to the parameter p_i is

$$\frac{\partial g^2_\mathbf{W}}{\partial p_i}(\mathbf{p}) = 2\Re \left\{ \left(\frac{\partial \mathbf{s}(\mathbf{p})}{\partial p_i} \right)^H \mathbf{W} \left(\mathbf{s}(\mathbf{p}) - \mathbf{s}^\mathrm{M} \right) \right\} . \tag{2.3}$$

In Eq. (2.3), the derivative of the scattering data $\mathbf{s}(\mathbf{p})$ with respect to parameters p_i are found from sensitivity expressions derived from Maxwell's equations. An example of a sensitivity expression for the scattering parameters with respect to permittivity is presented in Sec. 3.1.1. Sensitivities with respect to geometric shape and further details about gradient-based optimization are found in Refs. [18–20].

Gradient-based optimization is used in **Paper I** and the algorithm utilized is the sparse nonlinear optimizer (SNOPT) solver implemented in TOMLAB [21].

2.1.2 Linear Problems and Regularization

For small perturbations in the parameter vector $\mathbf{p}$ describing the scattering data, we can linearize our model of the scattering data using the gradient as

$$\mathbf{s}(\mathbf{p}) \approx \mathbf{s}(\mathbf{p}_i) + \nabla \mathbf{s}(\mathbf{p}_i) \delta \mathbf{p}_i \, . \tag{2.4}$$

where $\mathbf{p}_i$ is the linearization point. We find an estimated parameter perturbation $\delta \hat{\mathbf{p}}_i$ that describe the measured scattering data $\mathbf{s}^\mathrm{M}$ by solving the following quadratic minimization problem

$$\delta \hat{\mathbf{p}}_i = \arg \min_{\delta \mathbf{p}_i} ||\mathbf{A}_i \delta \mathbf{p}_i - \mathbf{b}_i||_2^2 + \gamma ||\mathbf{L}(\delta \mathbf{p}_i - \delta \tilde{\mathbf{p}}_i)||_2^2 \, , \tag{2.5}$$

where the sensitivity matrix $\mathbf{A}_i = \nabla \mathbf{s}(\mathbf{p}_i)$ relates the unknown perturbations $\delta\mathbf{p}_i$ in the parameters $\mathbf{p}_i$ to perturbations in the scattering data. Here, $\mathbf{b}_i = \mathbf{s}^{\mathrm{M}} - \mathbf{s}(\mathbf{p}_i)$ is the deviation of the measured scattering data compared to the model evaluated at the linearization point. Further, a regularization term is included in Eq. (2.5) and it penalizes deviations in $\delta\mathbf{p}_i$ far from the a priori specified values in $\delta\tilde{\mathbf{p}}_i$ using a weighted Euclidean norm. The minimization problem stated in Eq. (2.5) is a quadratic problem with regularization. However, the solution of this optimization problem can be expressed as an over-determined system of linear equations, which is derived by setting the derivative of the goal function in Eq. (2.5) to zero. We refer to the book by Engl et al. [22] for further details about regularization of inverse problems.

In **Paper III**, we construct a quadratic model similar to Eq. (2.5). It relates the perturbations in the resonant frequencies $\delta\boldsymbol{\omega}(\mathbf{p}_i)$ (around a linearization point) to the perturbations in the dielectric properties of a mixture inside a process vessel and the geometric shape of the vessel.

2.1.3 Databases

Given a measurement system, it can be advantageous to construct a database of the scattering data response and in some cases also the gradient of the scattering data. The database could, for example, be parameterized with respect to the dielectric properties of the unknown object and its size and position. Such a database can be used to analyze how well the measurement system is able to distinguish different parameter combinations. It could also be used as a look-up table to identify one (or several) parameter configurations that corresponds well to the measured scattering data. The parameter configuration found via the look-up procedure could then be used as an initial guess in a gradient-based optimization algorithm or as linearization point for a problem with small perturbations. Then, an optimization procedure could further improve on the estimated parameters, and even introduce additional degrees of freedom not parameterized in the database.

The computational cost of creating a database can be very high, since the number of computations typically scales exponentially with the number of parameters in the database. Moreover, the full electromagnetic problem must be solved for each parameter configuration and, often, for multiple frequencies. The construction of a database is, however, embarrassingly simple to parallelize using multiple computers in a cluster, since each computation is independent. Also, it is sufficient to compute and store the database once and, in subsequent uses of the database, we only need to load the stored data.

2.2 Classification

Classification is a broad subject with numerous methods and applications, where we refer to the book by Duda et al. [23] for an overview about statistical pattern classification and machine-learning. For classification in microwave systems, the goal is to find an automatized procedure to associate the measured scattering data $\mathbf{s}^{\mathrm{M}}$ with a class c, which is defined by a subset of the parameter space. Under the assumption that $\mathbf{s}^{\mathrm{M}}$ is well approximated by the physical model $\mathbf{s}(\mathbf{p})$, the classes could, for example, be represented by typical parameter vectors $\mathbf{p}_i^c$ for $i = 1, 2, \ldots$, where c denotes the class index. Further, we assume that the scattering data $\mathbf{s}(\mathbf{p}_i)$ spans a high-dimensional space $\mathbb{S}$, and the class specific scattering data $\mathbf{s}(\mathbf{p}_i^c)$ span a space $\mathbb{S}^c$, which is a subspace of $\mathbb{S}$. Therefore, we formulate a classification algorithm based on the assumption that each scattering data $\mathbf{s}(\mathbf{p}_i^c)$ for $i = 1, 2, \ldots$ in which the parameter vector $\mathbf{p}_i^c$ belong to class c is generated (possibly after some processing) according to a linear model defined as

$$\mathbf{s}(\mathbf{p}_i^c) = \mathbf{U}_c \boldsymbol{\alpha}_c^i + \mathbf{e}\,, \tag{2.6}$$

where $\mathbf{U}_c$ is a linear subspace basis that represents an approximation of the space $\mathbb{S}^c$, $\boldsymbol{\alpha}_c^i$ contains the weights of the basis vectors and $\mathbf{e}$ is additive white noise. The classifier decision of a new unlabeled scattering data point $\mathbf{s}(\mathbf{p}_i)$, is based on finding the minimum of the distances to the approximated subspaces, where the distance is computed via projection of $\mathbf{s}(\mathbf{p}_i)$ onto $\mathbf{U}_c$ using

$$d_c(\mathbf{s}(\mathbf{p}_i)) = ||\mathbf{s}(\mathbf{p}_i) - \mathbf{U}_c \mathbf{U}_c^H \mathbf{s}(\mathbf{p}_i)||_2\,. \tag{2.7}$$

The training of the classifier, i.e. determining $\mathbf{U}_c$, is based on singular value decomposition of a set of labeled data $\mathbf{s}(\mathbf{p}_i^c)$ for $i = 1, \ldots, N$.

In **Paper IV**, we use the above described classification algorithm for localization of intracranial bleedings. Here, the classes represent 10 different bleeding positions inside a patients head. We refer to **Paper IV** as well as Ref. [24] for further details about the subspace learning algorithm for microwave scattering classification.

CHAPTER 3

RESULTS

In this chapter, we test our parameter estimation methods (described in Sec. 2.1) on two microwave measurement systems that feature different electromagnetic characteristics: (i) an N-port reflection/transmission measurement system and (ii) a two-port resonance measurement system. Also, we provide some details on the electromagnetic modeling of these systems. Further, we discuss calibration procedures that use a reference case measurement. We continue with a brief overview of the results in the appended papers, where we first present results for permittivity estimation from measurements. Finally, we present results for two numerical studies in two different N-port systems. In the first study, we analyze the possibility of detecting variations from a constant material distribution using a database. In the second study, we characterize the performance of the classification algorithm presented in Sec. 2.2 for localization of intracranial bleedings.

3.1 Measurement Systems

We use two different microwave measurement systems to test our parameter estimation methods. The first measurement system is a 6-port prototype microwave tomography system for measurement of dielectric properties. The second measurement system is a monitoring system for a pharmaceutical process vessel. Here, the process vessel acts as a metal cavity and the interior resonances are exited using two H-probes. The estimated complex resonance frequencies are used for global and local monitoring of the permittivity inside the process vessel.

3.1.1 Microwave Tomography System

The system presented in **Paper I** and **Paper II** is a microwave tomography measurement system, where the measurement region is completely shielded from exterior disturbances by metal walls. In Fig. 3.1, we present a photograph of the tomography measurement system with network analyzer and switch as well as a photograph of the measurement region when the tomography measurement system is opened. The measurement region is a circular metal cavity formed by the intersection of six rectangular waveguides, which makes the cavity heavily loaded from an electromagnetic perspective by the waveguide apertures. Here, we measure the scattering parameters in a frequency band between 2.7 GHz and 5.1 GHz. By means of accurate electromagnetic modeling and gradient-based optimization as described in Sec. 2.1.1, we estimate the dielectric material properties (with uncertainties) of the material placed in the measurement region. In particular, we estimate the dielectric properties of microcrystalline-cellulose (MCC) pellets for different moisture contents.

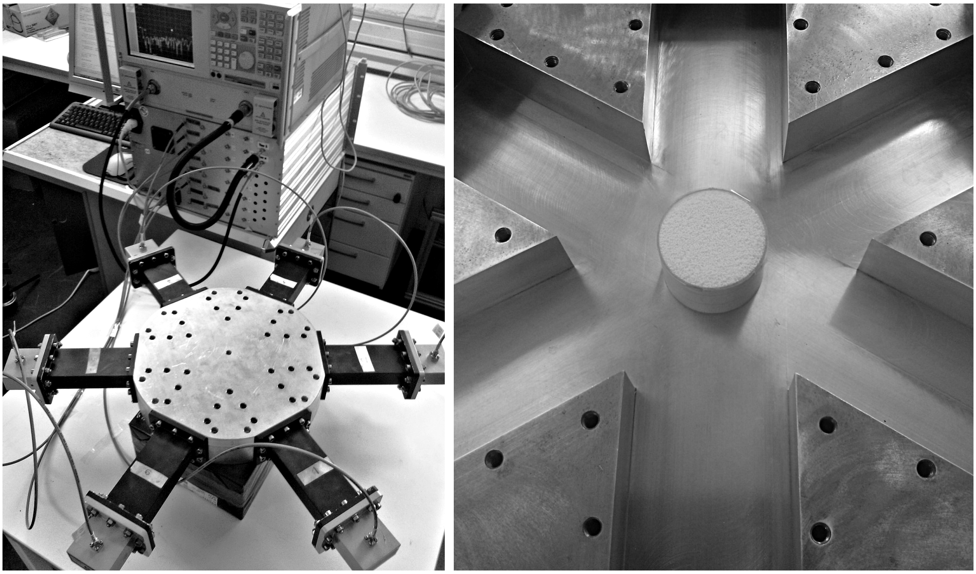

Figure 3.1: To the left, photograph of the prototype tomography measurement system with the network analyzer and switch used in **Paper I** and **Paper II**. To the right is a photograph of the measurement region of the opened tomography measurement system, where microcrystalline-cellulose (MCC) pellets are placed in a plastic holder.

For microwave measurement systems such as the tomography system, it is sufficient to analyze a two-dimensional slice as presented in Fig. 3.2. In this type of geometry, Maxwell's equations can be reduced to two independent Helmholtz equations. These equations correspond to the two different polarizations commonly described as transverse electric (TE) and transverse magnetic (TM). This decomposition is only valid for material distributions that are well described as a right generalized cylinder[1], i.e. the material distribution must be uniform along the z-direction.

[1]A generalized cylinder is a ruled surface parameterized as $\vec{r}(u, v) = v\vec{r}_0 + \vec{r}_s(u)$ where $\vec{r}_0$ is a fixed point and $\vec{r}_s(u)$ is a curve [25]. We denote the cylinder right if $\vec{r}_0 \perp \vec{r}_s(u)$.

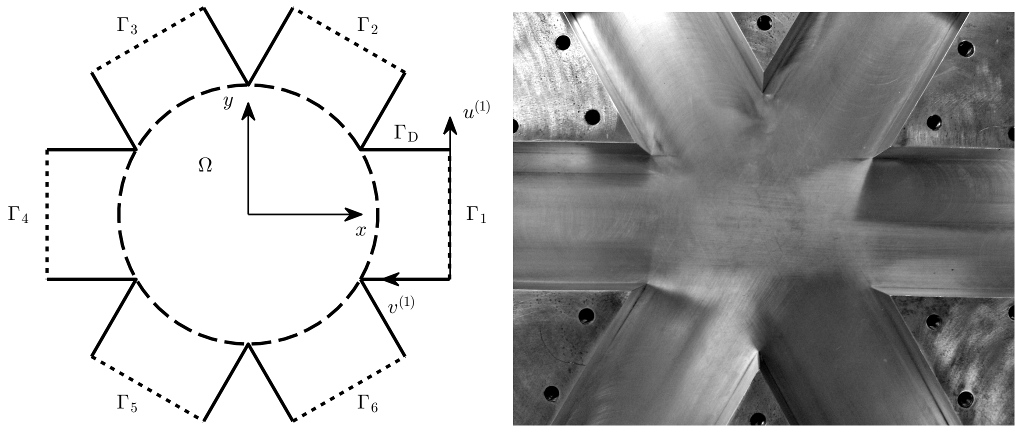

Figure 3.2: To the left, a two dimensional geometry representation of the tomography measurement system. The region inside the dashed circle is referred to as the measurement region. The dotted lines represent waveguide port boundaries and the solid line metal walls. To the right, a photograph of the (opened) tomography measurement system.

The TM polarization[2] for the geometry in Fig. 3.2 is described by

$$-\nabla^2 E_z - \omega^2 \mu_0 \epsilon E_z = 0 \qquad \text{in } \Omega \tag{3.1a}$$

$$E_z = 0 \qquad \text{on } \Gamma_{\mathrm{D}} \tag{3.1b}$$

$$\hat{\boldsymbol{n}} \cdot \nabla E_z + jk_{\mathrm{wg}} E_z = 2jk_{\mathrm{wg}} E_{0z,p}^{+} \qquad \text{on } \Gamma_p, \quad p = 1, \ldots, 6 \tag{3.1c}$$

where all waveguides are identical[3] and k_{wg} is the waveguide wavenumber for each waveguide. Here, $E_{0z,p}^{+}$ is the incident field amplitude of the fundamental mode for port p. We refer to the book by Pozar [26] for further details about waveguides and modes. Eq. (3.1) with only one non-zero incident amplitude for one of the waveguide ports yields the reflection coefficient at this port as well as the transmission coefficients to all other ports. By consecutive excitation of one port at a time, while the other ports are measured (and impedance matched), we construct the scattering matrix $\mathbf{S}$ that describes all possible reflection and transmission coefficients of the measurement system. This scattering matrix is mainly dependent on the geometry of the structure but also on the material distribution $\epsilon = \epsilon(\vec{r}, \omega)$ inside the measurement region. By an adjoint field formulation [18], it is possible to derive sensitives that relate perturbations $\delta\mathbf{S}$ in the scattering matrix to

[2] Note that the propagation direction is not in the z-direction, as is common practice for waveguide structures. Here, the field is propagating in the xy-plane. We denote this case as the TM polarization simply because we have no z-component of the magnetic field.

[3] The waveguides width and height are equal, as well as the homogeneous material filling the interior of the waveguides.

perturbations $\delta\epsilon$ in the material distribution according to

$$\delta S_{p,q} = \frac{\omega^2 \mu_0}{2jk_{\mathrm{wg}} \mathrm{w}_{\mathrm{wg}} E^{+}_{0z,p} E^{+}_{0z,q}} \int_{\Omega} \delta\epsilon E_{z,p} E_{z,q} \, \mathrm{d}\Omega \,, \tag{3.2}$$

where w_{wg} is the waveguide width. Moreover, $E_{z,p}$ is the field when port p is excited (the adjoint problem) and $E_{z,q}$ is the field when port q is excited (the original problem). We note that Eq. (3.2) does not require the computation of a new field solution since all ports has to be excited once in order to compute the entire scattering matrix.

In **Paper IV**, we present a numerical study of a measurement helmet system in which microwaves are used for localization of intracranial bleedings. In the numerical study, the measurement system is simplified to a two-dimensional problem. Here, 8 waveguides are positioned around the patients head and water bags are placed in between the skull and the waveguide openings to increase the coupling of the electromagnetic wave into the head. In this study, the TE polarization is used and the corresponding field problem is similar to the TM polarization (3.1).

3.1.2 Monitoring of a Pharmaceutical Process Vessel

In **Paper III**, a resonance measurement system is presented for global and local monitoring of a pharmaceutical process vessel. Fig. 3.3 shows a photograph of the pharmaceutical process equipment with the cylindrical process vessel and the two H-probes that are used to excite the resonances. Here, the objective is to monitor the material moisture content and its distribution inside the process vessel during operation, where the purpose is to ensure a high quality output product and minimize the risk of a batch reject due to agglomeration. The process vessel is loaded with MCC pellets that are fluidized by air during operation. These pellets are coated by an aqueous solution that is sprayed onto the pellets, and they are subsequently dried. Here, we estimate multiple resonant frequencies between 0.7 GHz and 1.5 GHz from the measured scattering parameters by means of a subspace-based identification algorithm [16]. By means of material-based sensitives, a quadratic optimization problem with regularization (as described in Sec. 2.1.2) is used to estimate the material parameters for three different sub-regions inside the vessel.

For closed metal vessels, the resonant phenomena can be described by the eigenvalue problem

$$\nabla \times \nabla \times \boldsymbol{E} - \omega^2 \mu_0 \epsilon \boldsymbol{E} = \boldsymbol{0} \qquad \text{in } \Omega \tag{3.3a}$$

$$\hat{\boldsymbol{n}} \times \boldsymbol{E} = \boldsymbol{0} \qquad \text{on } \Gamma \tag{3.3b}$$

where Ω denotes the interior region of the metal vessel and Γ its metal walls. The material distribution inside the vessel is characterized by the permittivity $\epsilon = \epsilon(\vec{r}, \omega)$. The eigenvalue problem (3.3) yields pairs of eigenfrequencies ω_i and eigenmodes $\boldsymbol{E}_i$, where i is an integer index. This solution depends mainly on the dimensions of the metal vessel, but also on the material distribution inside the vessel. The dependence of the eigenfrequencies on the material distribution in combination with perturbation theory [27], yields sensitivities that relate perturbations $\delta\omega_i$ of the resonant frequencies

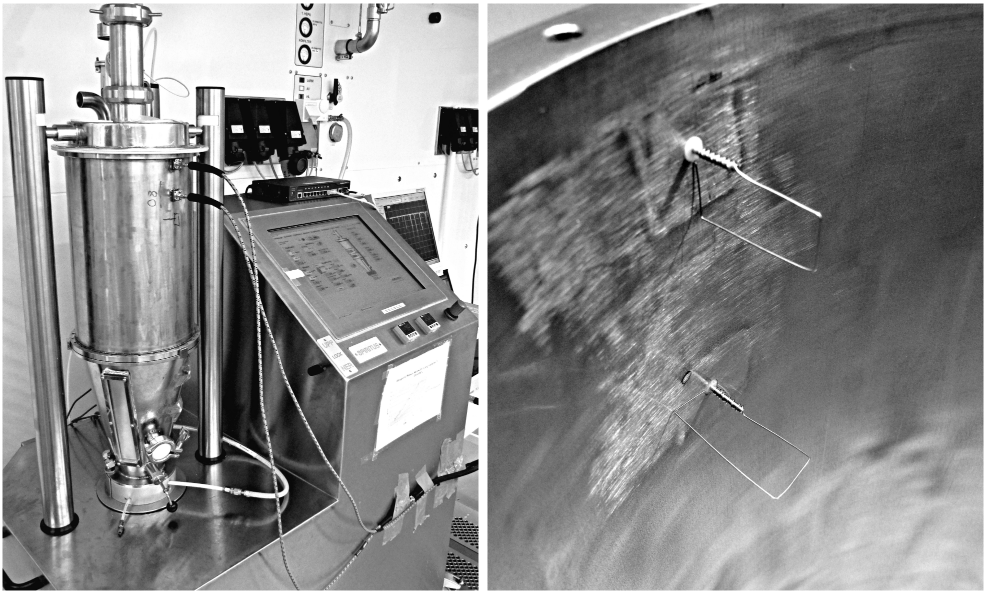

Figure 3.3: To the left, photograph of the pharmaceutical process vessel presented in detail in **Paper III**. To the right, the mounted H-probes used to excite the microwave resonances inside the vessel.

to the corresponding perturbations $\delta\epsilon$ in the material distribution. For further details in the derivation of sensitivities, the reader is referred to **Paper III**.

3.1.3 Comparison Between Measurements and Simulations

In general, microwave measurement systems suffer from various sources of measurement errors, such as noise and geometrical details that can be difficult to model. Further, the measurement systems are often non-stationary in time, due to for example temperature variations and cable flexing/displacements. A simulation model is in general an idealization of the measurement system based on a number of simplifications such as (i) all the physical dimensions of the measurement system are assumed to be known, (ii) geometrical defects of the system are neglected and (iii) the measuring device (e.g. network analyzer and cables) is often completely removed or simplified. In addition to the calibration of the measuring device, a second calibration or modeling scheme is often used to remove part of the deficiencies of the measurement system compared to the simulation model. An example of such a calibration is the cancellation of phase variation between the measurement data and the simulated data based on a reference case measurement [28]. For scattering data, we could use $\mathbf{s}^{\mathrm{M}}_{\mathrm{cal}} = (\mathbf{s}(\mathbf{p}_{\mathrm{ref}})./\mathbf{s}^{\mathrm{M}}_{\mathrm{ref}}). \times \mathbf{s}^{\mathrm{M}}$ as the calibrated measurement data, where element-wise division and multiplication is denoted $./$ and $.\times$, respectively. In an alternative approach, we could compare the deviations of the measured and simulated data against a reference case, such as $\Delta\mathbf{s}^{\mathrm{M}} = \mathbf{s}^{\mathrm{M}} - \mathbf{s}^{\mathrm{M}}_{\mathrm{ref}}$ and $\Delta\mathbf{s}(\mathbf{p}) = \mathbf{s}(\mathbf{p}) - \mathbf{s}(\mathbf{p}_{\mathrm{ref}})$. The calibrated measurement data could then expressed as $\mathbf{s}^{\mathrm{M}}_{\mathrm{cal}} = \mathbf{s}^{\mathrm{M}} - \mathbf{s}^{\mathrm{M}}_{\mathrm{ref}} + \mathbf{s}(\mathbf{p}_{\mathrm{ref}})$.

In the tomography measurement setup described in Sec. 3.1.1, we try to remove unmodeled effects from our measured scattering parameters $\mathbf{s}^{\mathrm{M}}$ using an estimation of the unmodeled coaxial cable to waveguide adapters, where the adapters can be seen in Fig. 3.1. The adapters are not included in our simulation model[4] and in our modeling scheme, we estimate the adapters characteristics and remove their effect on the scattering parameters by means of a reference case[5] measurement. Here, we assume that the six adapters are identical 2-port systems, described by the same 2-by-2 scattering matrix $\mathbf{S}^{\mathrm{a}}$, see **Paper I** for the details. We find that using this modeling scheme as our calibration, we achieve a residual of about -30 dB between our simulated and measured scattering matrices as a function of frequency. In Fig. 3.4, we present the amplitude of the estimated adapter scattering parameters, as well as the amplitude of the measured, calibrated and simulated reflection coefficient for the first port of the tomography measurement system for the reference case. We find that this modeling scheme is robust, the achieved residual as a function of frequency for subsequent measurements of the reference case is almost stable with respect to time (over the course of a day) and to opening/closing of the measurement system.

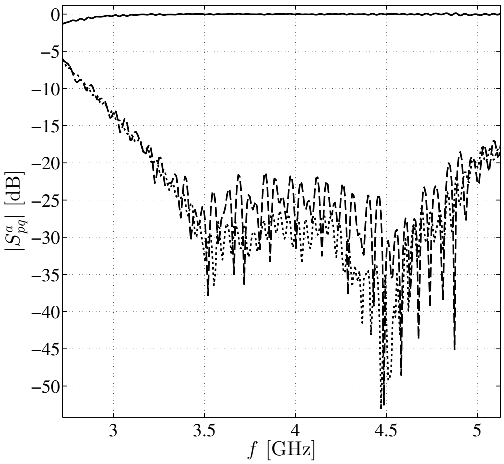

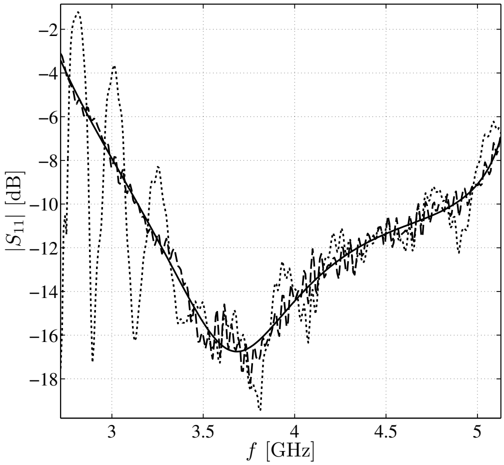

Figure 3.4: To the left, the amplitude of the estimated adapter scattering parameters as a function of frequency. Here, the solid line represents S^{a}_{12} and S^{a}_{21}, dotted S^{a}_{11} and dashed S^{a}_{22}. To the right, the amplitude of the measured reflection for the first port of the prototype measurement system is shown for the reference case ($S_{11,\mathrm{ref}}$). Here, the solid line represents simulated scattering data, dotted measured scattering data and dashed calibrated (via removal of adapters) measured scattering data.

For the monitoring system described in **Paper III**, we also remove some discrepancies between our simulation model and our measurement system, as well as some unmodeled effects (e.g. metal conductivity, geometric defects etc.). In detail, we compare the relative resonant frequency shifts $\Delta\omega_i^{\mathrm{M}} = (\omega_i^{\mathrm{M}} - \omega_{i,\mathrm{ref}}^{\mathrm{M}})/\omega_{i,\mathrm{ref}}^{\mathrm{M}}$ between our measurements and

[4]To model the adapters we need a three dimensional model.

[5]The reference case is specified as the case with an empty measurement region.

our simulation model for some resonant frequencies $i = 1, \ldots, N$. The reference case is here the empty measurement system at room temperature. Measurements for the reference case are done at the start of the process operation by a series of measurements before the process vessel is loaded with MCC pellets. The deviations in subsequent measurements of the resonant frequencies from this initial state are then modeled via the corresponding deviations in our system model. Here, we can estimate variations in the complex permittivity due to changes in $\Delta\omega_i^{\mathrm{M}}$ on the order of ppm. In **Paper III**, we also present the measured and simulated resonant frequencies and find that they agree well[6]. This agreement shows that our physical model is in good agreement with the measurement setup. In the monitoring system, we have access to temperature measurements during the process time. Temperature variations alter the size and shape of the metal vessel, which in turn affect the resonant frequencies. However, this temperature information is assumed a priori known and incorporated in the parameter estimation problem via regularization.

3.2 Permittivity Estimation from Measurements

The tomography measurement system described in Sec. 3.1.1 is used to estimate the dielectric properties of materials. To estimate the dielectric properties of a material in the tomography system, we position a sample (of equal height to the waveguides) inside the measurement region. Here, we find the following result; if an acrylic glass cylinder is positioned at the center of the measurement region and we jointly optimize both the radius and the permittivity of the cylindrical sample, we find by analyzing the goal function an ambiguity between the size and permittivity of the sample. In Fig. 3.5, we present a photograph where an acrylic glass cylinder is positioned at the center of our measurement region, and a contour plot of the RMSD[7] between the calibrated measurement data versus simulated data. In the simulated data, a circular cylinder is positioned at the center of the measurement region and a database of the scattering response constructed. Here, the database is parameterized with respect to the cylinder radius a and relative permittivity ϵ_r. We can see in the contour plot in Fig. 3.5 that the region with below -28 dB agreement between the measured and simulated data is a large elongated region. There is no clear global minima defined, and according to the used database, any permittivity/radius combination inside the -28 dB envelope would be a good fit given the noise level of our measurement data.

Ambiguity in scatterer permittivity versus size is not unexpected for microwave measurement systems when the wavelength is large compared to the sample size. A simple example is the induced dipole moment of a dielectric sphere of size D when illuminated by a plane wave with wavelength $\lambda \gg D$. Here, the induced dipole moment is proportional

[6]We find deviations of the order of a few MHz, yielding relative error on the order of 10^{-4}. We have larger deviations in the imaginary part of the resonant frequencies due to larger differences in the simulated and computed Q values.

[7]The root-mean-square deviation (RMSD) in dB is computed as $20\log_{10}\sqrt{g^2_{\mathbf{W}_0}}$ for $g^2_{\mathbf{W}}$ defined in Eq. (2.2).

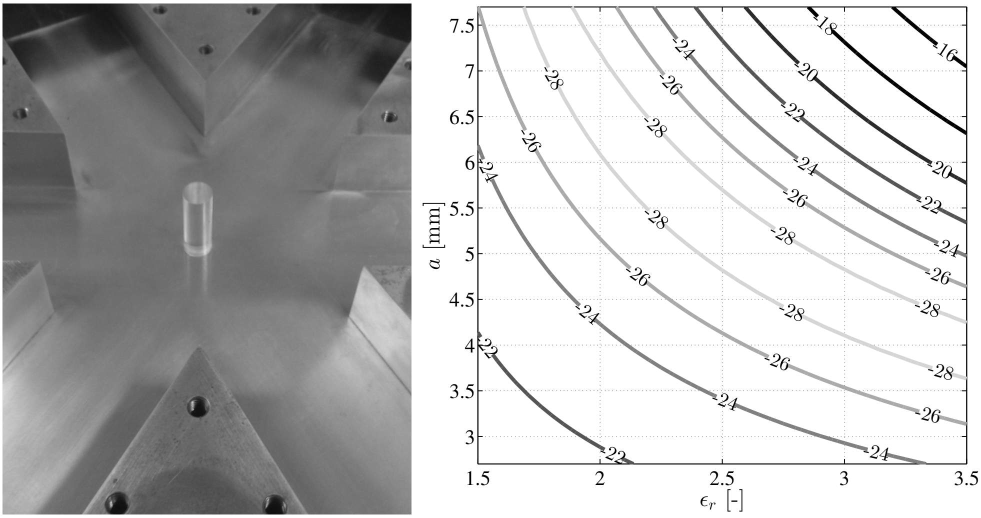

Figure 3.5: To the left, photograph of an acrylic glass cylinder (radius 5.2 mm) positioned at the center of the measurement domain of the (opened) tomography measurement system. To the right, contour plot in dB of the RMSD between the calibrated measurement data for the the acrylic glass cylinder and simulated data of a circular cylinder positioned in the center and parameterized with radius a and relative permittivity ϵ_r.

to $(\epsilon_r - 1)/(\epsilon_r + 2)V$, where V is the sphere volume [29]. The induced dipole moment describes the scattered field, and we find that both ϵ_r and V can be varied in such a manner that the dipole moment is unchanged. If the frequency is increased sufficiently ($\lambda \approx D$), higher-order dipole moments are induced, and we have a greater possibility of resolving the ambiguity between size and permittivity.

For the results presented in Fig. 3.5, we utilized 200 frequency points in the frequency band between 2.7 GHz and 5.1 GHz and measured/illuminated the sample from six different directions. Here, λ is approximately 12 to 24 times the radius of the acrylic glass cylinder. In the tomography system, we can not resolve the permittivity/size ambiguity and it could be difficult in other microwave measurement systems to resolve similar ambiguities using only the available frequencies and/or number of sensors. A complimentary approach to remove or mitigate problems related to the ambiguities of this type is to include a priori information. For example, we could assume that the sample size is known a priori to completely remove the ambiguity problem in Fig. 3.5. Other approaches could be to only allow certain permittivity values or geometric shapes such as in Ref. [30].

In **Paper I**, we estimate the relative permittivity of the acrylic glass cylinder[8] (where we assume that the sample radius is known a priori) to $\epsilon_r \approx 2.54 \pm 0.06$ in the tomography system, which can be compared to $\epsilon_r \approx 2.62 \pm 0.09$ in a cylindrical cavity via a cavity perturbation technique. These results agree well and we conclude that our tomography measurement system can accurately measure dielectric properties. We have also analyzed

[8] We also have preliminary estimates of the acrylic glass cylinders permittivity presented in **Paper II**. The deviations are due the new calibration method presented in **Paper I**.

the positioning capabilities of the tomography measurement system. In simulations, we find that a movement of the acrylic glass cylinder less than 5 mm from the center of the measurement region resulted in RMSD between the scattering parameters that is smaller than -30 dB. Thus, we could expect a positioning measurement accuracy of about 5 mm in the tomography system. Preliminary results show that using a database parameterized with position, we find that the estimated positions of the acrylic glass cylinder based on microwave measurements are within 1-2 mm from the actual position measured geometrically with a ruler.

3.2.1 Complex Permittivity of Densely Packed MCC Pellets

We continue to use the microwave tomography system presented in Sec. 3.1.1 to estimate the effective permittivity of densely packed MCC pellets in **Paper I**. We estimate the dielectric properties for four different batches of MCC pellets with increasing moisture content for four different dispersion models. In Fig. 3.6, we present the estimated real and imaginary part of the complex relative permittivity as a function of frequency for the MCC/air mixture. Here, four different moisture contents of the MCC pellets are analyzed and the estimated permittivity using the Debye, Cole-Cole and Cole-Davidsson models[9] presented.

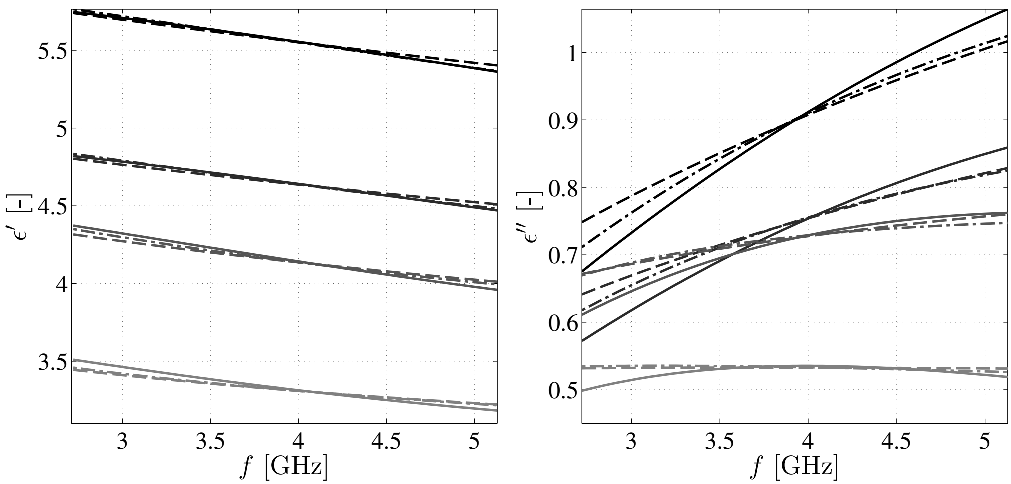

Figure 3.6: Real and imaginary part of the complex relative permittivity ($\epsilon_c = \epsilon' - j\epsilon''$) for four different batches of MCC pellets. Here, the color shades black to gray corresponds to 22.8%, 16.8%, 12.2% and 9.2% moisture content, respectively. Solid lines represents a Debye dispersion model, dashed Cole-Cole and dashed-dotted Cole-Davidsson.

In Tab. 3.1, we present the estimated Debye-parameters with uncertainties computed from a sensitivity analysis around the optima. Uncertainties in the measured holder posi-

[9]We have for the Debye model that $\epsilon(\omega) = \epsilon_0(\epsilon_\infty + \frac{\epsilon_s - \epsilon_\infty}{1+j\omega\tau})$, see **Paper I** for the Cole-Cole and Cole-Davidsson models.

tion, size and relative permittivity, as well as an estimate of the noise in the measurement system are propagated via their respective sensitivities to uncertainties in the optimized parameters.

Table 3.1: Estimated Debye parameters with uncertainties for four different batches of MCC pellets with different moisture content (MC).

MC [%]	ϵ_s	ϵ_∞	τ [ps]
9.2	3.62 ± 0.02	2.63 ± 0.03	32.0 ± 0.9
12.2	4.27 ± 0.03	2.85 ± 0.04	24.2 ± 0.8
16.8	4.88 ± 0.05	2.79 ± 0.12	15.5 ± 0.7
22.8	5.49 ± 0.07	2.36 ± 0.26	10.3 ± 0.7

3.2.2 Estimation and Monitoring of Permittivity Distribution

Paper III presents a microwave measurement system for the monitoring of a pharmaceutical process vessel. Here, we estimate the complex relative permittivity of three different sub-regions inside the vessel by measuring the complex resonant frequencies. In the process vessel, a batch of 200 grams of MCC pellets are fluidized by injection of air forming a boiling bed region in the bottom section of the process vessel. In the bed region, the homogenized relative permittivity is significantly higher than in the remainder of the process vessel as the density of MCC particles is high. A fraction of the MCC pellets are in addition accelerated by a spray nozzle such that they move in a fountain like pattern inside the vessel. At the center of the fountain region, we assume that there is a cylindrical region with moderate particle density. This cylindrical representation of the fountain is our second sub-region. The third sub-region is selected as the remainder of the vessels interior volume, which presumably has a very low particle density.

During typical operation of the process vessel the MCC pellets are coated by spraying an aqueous solution. In Fig. 3.7, the estimated relative permittivity is shown for the bed and fountain region, when coating the MCC pellets with a solution containing Mannitol and Kollicoat IR® at a low spraying rate. We can see that the estimated permittivity in the bed region increases during the spraying interval, which could be explained by that the particles grow in size as a result of the coating. The growth of the particles due to coating was verified by means of weighing after the process was completed. In the estimated permittivity of the fountain region, we can clearly see when the fountain is switched on. In **Paper III**, we also present scatter plots of the estimated complex permittivities and we find that measurements taken at different time instants fall approximately on a straight line. Further, we find that the slope of this line, which corresponds to the electric loss tangent $\tan \delta_\epsilon = \epsilon''/\epsilon'$, significantly increases when we spray the particles with a solution featuring large dielectric losses.

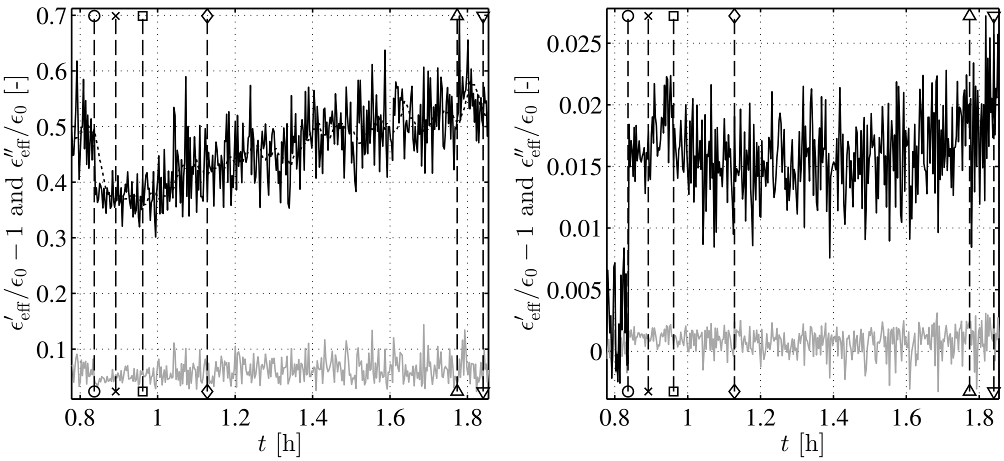

Figure 3.7: Coating of MCC pellets with low spray rate (6.6 g/min). Estimated $\epsilon' - 1$ in black and ϵ'' in gray for the bed region to the left and the fountain region to the right. At the vertical dashed line equipped by circle glyphs, the fountain is switched on. At subsequent glyphs (cross and square) the spray rate is increased successively. The diamond glyph represent when temperature variations are relatively small. At the triangle glyph the spraying was stopped.

3.3 Detection of Variations in Material Distribution

In **Paper II**, a numerical study is performed to analyze the possibility of detecting bubbles/agglomerations in a homogenized background representing fluidized MCC pellets. Here, a setup similar to the experimental tomography system is utilized which could be mounted for monitoring of the lower (bed) region of the pharmaceutical process vessel presented in Sec. 3.1.2. In a parameter study, we construct a database with the scattering response evaluated on a coarse grid that parameterize the problem with respect to bubble location, size, relative permittivity, conductivity as well as the backgrounds dielectric properties. We find that given an artificial measurement for the scattering data, a look-up procedure yields reasonably close parameter values to the ground truth if the scattering data is sufficiently close to a grid point in the database. We believe the database approach could be significantly improved if an interpolation scheme between the database grid points is employed. Further, the parameter values that are identified from the database could be used as the initial guess to a gradient-based optimization algorithm.

3.4 Localization of Bleedings via Classification

Paper IV describes a numerical study of a simplified version of a measurement system for localization of traumatic intracranial bleedings. The goal is to classify, based on measured scattering data, if and where a bleeding is located inside the head of a patient.

Here, we use the subspace based classification algorithm described in Sec. 2.2. To analyze the performance of such a classifier, we find that electromagnetic simulations is a useful tool to generate a large number of labeled signal data for testing purposes.

In **Paper IV**, we train the classification algorithm and validate it on an independent data set to analyze its accuracy. The training set contains 10 different classes corresponding to different bleeding locations. To model patient variability in the training data, we vary head size by $\pm 6\%$, head position[10] as well as the thickness of the bleedings from 0.2 cm to 2.5 cm. A five-fold cross validation is used to analyze the accuracy of the classifier for 100 different observations. We find that the classifier correctly identifies each position for at least 94% of the observations and that, in all cases but one, it determines the position as either the correct or the (geometrically) second closest position. Given an observation for a known position, we also note that the subspace distance to classes representing an adjacent position is in general much smaller than the distance to classes representing positions geometrically further away.

[10]The head position was parameterized by a $\pm 6^\circ$ rotation versus the antenna array.

CHAPTER 4

CONCLUSION

In the context of microwave measurement systems, this thesis presents a number of algorithms for parameter estimation and classification. Measurements for a reference case are used to (i) establish experimentally determined models for parts of the system and/or (ii) calibrate the model with respect to the experimental equipment. Further, we minimize a goal function that describes the misfit between (i) the measured system response and (ii) a model of the measurement system that depends on a set of parameters to be determined. In particular, we use (i) gradient-based optimization on a transmission/reflection measurement system, (ii) minimization of a quadratic goal function with regularization for a resonance measurement system and (iii) a classification algorithm that exploits computed databases. Here, the databases can be used as look-up tables or as training data for the (subspace based) classification algorithm. Further, the physical models of the measurement systems are based on accurate electromagnetic models using the finite element method.

We employ parameter estimation using gradient-based optimization for a 6-port transmission/reflection microwave tomography measurement system. Here, the misfit between the measured scattering parameters and the physical model of the scattering parameters is minimized. In particular, we characterize the complex relative permittivity of densely packed microcrystalline-cellulose (MCC) by means of four different dispersion models for frequencies between 2.7 GHz and 5.1 GHz. For situations when the object size is substantially smaller than the wavelength, we find that our parameter estimation problem becomes ill-posed, and we incorporate the object size as a priori information to mitigate this problem. For the densely packed MCC pellets, we find that the estimated permittivity for the different material models agree well and that the estimated permittivity depends on the moisture content. Additionally, the tomography system is used to estimate the relative permittivity of an acrylic glass cylinder, and the result are in good agreement with measurements from a cylindrical cavity resonator. The calibration scheme, in which we also model the coaxial to waveguide adapters, is robust with respect to opening/closing the system and we typically achieve a residual of -30 dB between simulated and measured scattering data.

We form a quadratic optimization problem with regularization for a resonance measurement system used for monitoring of a pharmaceutical process vessel. Here, we exploit that the vessel is a closed metal cavity and measure its complex resonant frequencies. Small variations in the resonant frequencies are related by sensitivities to small variations in the complex permittivity and in the cavity shape. The regularization allows for the incorporation of a priori temperature measurement information, which affects the cavity size and shape. In particular, we load the vessel with 200 grams of MCC pellets and execute a number of process steps. During the process, the MCC pellets are coated with an aqueous solution and subsequently dried. In the final application, the moisture content of the MCC pellets is important to monitor to assure a high quality output product. From the measured relative resonance shift, we estimate the complex relative permittivity as a function of process time for three different sub-regions inside the vessel: (i) the bed, (ii) the fountain and (iii) the remainder of the volume. During a coating process at a low spray rate, we find that the permittivity of the bed region increase.

In a numerical study with a geometry similar to the tomography system, we analyze the possibility of detecting inhomogenities in a fluidized bed of MCC pellets. A look-up procedure for a coarse database parameterized with respect to background and inclusion properties (e.g permittivity, conductivity, position, size etc.) yields reasonable estimates if the scattering data is sufficiently close to a precomputed grid point in the database. In addition, the identified parameter combination in the database could be used as an initial guess for a gradient-based optimization algorithm.

Finally, we present a numerical study of a simplified microwave measurement system for the localization of intracranial bleedings. Here, we train a subspace based classifier and find that it is well-suited for classification of different bleeding positions. We subject our simulated data to patient variability (e.g. head size, orientation, bleeding size), and the classifier correctly classifies at least 94% of the observations in a five-fold cross validation.

REFERENCES

[1] E. Nyfors and P. Vainikainen, “Industrial microwave sensors,” *1991 IEEE MTT-S International Microwave Symposium Digest*, 1991.

[2] A. Toropainen, P. Vainikainen, and E. Nyfors, “Microwave Humidity Sensor for Difficult Environmental Conditions,” *17th European Microwave Conference, 1987*, 1987.

[3] G. B. Gentili, C. Riminesi, and V. Tesi, “Low Cost Microwave Sensor for Moisture Content Measurement in Paper Milling Industry,” *Sensing and Imaging: An International Journal*, vol. 7, pp. 155–173, Dec. 2006.

[4] N. Nikolova, “Microwave imaging for breast cancer,” *Microwave Magazine, IEEE*, no. November, pp. 78–94, 2011.

[5] S. Y. Semenov and D. R. Corfield, “Microwave Tomography for Brain Imaging: Feasibility Assessment for Stroke Detection,” *International Journal of Antennas and Propagation*, vol. 2008, pp. 1–8, 2008.

[6] D. W. Winters, J. D. Shea, P. Kosmas, B. D. Van Veen, and S. C. Hagness, “Three-dimensional microwave breast imaging: dispersive dielectric properties estimation using patient-specific basis functions.,” *IEEE transactions on medical imaging*, vol. 28, pp. 969–81, July 2009.

[7] A. E. Bulyshev, A. E. Souvorov, S. Y. Semenov, V. G. Posukh, and Y. E. Sizov, “Three-dimensional vector microwave tomography: theory and computational experiments,” *Inverse Problems*, vol. 20, pp. 1239–1259, Aug. 2004.

[8] D. K. Cheng, *Field and Wave Electromagnetics*, vol. 2. Addison Wesley, 2nd ed., 1989.

[9] J. C. Maxwell, “A Dynamical Theory of the Electromagnetic Field,” *Philosophical Transactions of the Royal Society of London*, vol. 155, pp. 459–512, 1865.

[10] A. Bondeson, T. Rylander, and P. Ingelström, *Computational Electromagnetics.* Springer, 2nd ed., 2012.

[11] K. Yee, "Numerical solution of initial boundary value problems involving Maxwell's equations in isotropic media," *IEEE Transactions on Antennas and Propagation*, vol. 14, pp. 302–307, 1966.

[12] R. F. Harrington, "Field Computation by Moment Methods," *Power*, vol. 10, pp. 2–3, 1993.

[13] J. C. Nédélec, "Mixed finite elements in R3," *Numerische Mathematik*, vol. 1, no. 35, pp. 315–341, 1980.

[14] J. Jianming, *The Finite Element Method in Electromagnetics.* Wiley-IEEE Press, 2nd ed., 2002.

[15] R. C. Aster, B. Borchers, and C. H. Thurber, *Parameter Estimation and Inverse Problems.* Academic Press, 2nd ed., 2013.

[16] T. McKelvey, H. Akçay, and L. Ljung, "Subspace-based multivariable system identification from frequency response data," *IEEE Transactions on Automatic Control*, vol. 41, no. 7, pp. 960–979, 1996.

[17] J. J. E. Dennis and R. B. Schnabel, *Numerical Methods for Unconstrained Optimization and Nonlinear Equations.* Soc for Industrial & Applied Math, 1996.

[18] A. Bondeson, Y. Yang, and P. Weinerfelt, "Optimization of Radar Cross Section by a Gradient Method," *IEEE Transactions on Magnetics*, vol. 40, pp. 1260–1263, Mar. 2004.

[19] T. Halleröd, D. Ericsson, and A. Bondeson, "Shape and material optimization using gradient methods and the adjoint problem in time and frequency domain," *COMPEL: The International Journal for Computation and Mathematics in Electrical and Electronic Engineering*, vol. 24, no. 3, pp. 882–892, 2005.

[20] P. Jacobsson and T. Rylander, "Gradient-based shape optimisation of conformal array antennas," *IET Microwaves, Antennas & Propagation*, vol. 4, no. 2, p. 200, 2010.

[21] K. Holmström, "The TOMLAB Optimization Environment in Matlab," 1999.

[22] H. W. Engl, M. Hanke, and A. Neubauer, *Regularization of Inverse Problems*, vol. 375. Dordrecht: Springer Netherlands, 1996.

[23] R. O. Duda, P. E. Hart, and D. G. Stork, *Pattern Classification.* Wiley, 2000.

[24] Y. Yinan and T. McKelvey, "A subspace learning algorithm for microwave scattering signal classification with application to wood quality assessment," in *IEEE International Workshop on Machine Learning for Signal Processing*, no. 3, pp. 1–6, Sept. 2012.

[25] E. W. Weisstein, *Generalized Cylinder.* From MathWorld – A Wolfram Web Resource, 2014.

[26] D. M. Pozar, *Microwave Engineering.* Willey, 4th ed., 2011.

[27] M. Dressel, O. Klein, S. Donovan, and G. Grüner, "Microwave cavity perturbation technique: Part III: Applications," *International Journal of Infrared and Millimeter Waves*, vol. 14, pp. 2489–2517, Dec. 1993.

[28] A. Fhager, M. Gustafsson, and S. Nordbo, "Image reconstruction in microwave tomography using a dielectric Debye model," *IEEE Transactions on Biomedical Engineering*, vol. 59, pp. 156–66, Jan. 2012.

[29] A. J. Stratton, *Electromagnetic Theory.* John Wiley & Sons, 2007.

[30] A. Fhager and M. Persson, "Using a priori data to improve the reconstruction of small objects in microwave tomography," *IEEE transactions on microwave theory and techniques*, vol. 55, no. 11, pp. 2454–2462, 2007.